DNA-like Photophysics in Self-Assembled Silver(I)-Nucleobase Nanofibers

Joshua A. Snyder, Aaron P. Charnay, Forrest R. Kohl, Yuyuan Zhang and Bern Kohler*

Department of Chemistry and Biochemistry, The Ohio State University, 100 West 18th Avenue, Columbus, Ohio 43210, United States

Author Information

Corresponding Author
* Bern Kohler. E-mail: kohler.40@osu.edu. Tel: +1 614-688-2635.

ORCID
Bern Kohler: 0000-0001-5353-1655
Joshua Snyder: 0000-0001-7818-1014

Abstract

Supramolecular assemblies form when silver nitrate is added to an aqueous solution of adenine (Ade) or 2-aminopurine (2AP) in a 2:1 mole ratio. Atomic force microscopy (AFM) images reveal nanofibers that are ~30 nm in diameter and micrometers in length in the dried film formed from a room-temperature solution. Femtosecond broadband transient absorption spectroscopy was used to investigate the dynamics of excited states formed by UV excitation of the nanofibers at room temperature aqueous solutions in an effort to learn how nonradiative decay pathways of the uncomplexed nucleobases are altered in the silver ion-mediated assemblies. The changes in the spectroscopy and dynamics of Ade and 2AP upon forming nanofibers with silver ions closely parallel ones seen when these bases are organized into DNA strands. The similarities strongly suggest that these structures feature extensive π-π stacking interactions between nucleobases. The results show that time-resolved spectroscopy combined with growing understanding of the photophysics of DNA strands can deliver new insights into the properties of metal-nucleobase nanoassemblies.

Introduction

The biological effects of metal ion binding to DNA have been of interest for many years, but there is growing interest in the supramolecular structures and nanomaterials that form by self-assembly when metal ions coordinate to nucleobases.[1-9] The base pairs in double-stranded DNA can bind small numbers of Ag^+ ions, which can then be reduced to form Ag nanoclusters (AgNCs).[10-16] The emission of these clusters is widely tunable from the visible to the NIR and is of interest for biomedical imaging.[17-21] Because the nucleobases are polydentate ligands that combine prolifically with Ag^+ ions, they can also form coordination oligomers and polymers,[22-24] which can readily assemble into different kinds of nanostructures even though the nucleobases are not linked in strands.[1-9] Imaging techniques such as atomic force microscopy (AFM) and electron microscopy have revealed morphological properties on the scale of nanometers,[1-9] but the molecular-level structural motifs remain unclear. The soft matter nanostructures that are of interest may be difficult to crystallize, or there may be uncertainty about whether the observed crystal structures capture ones actually present in aqueous solution.

Here, we use femtosecond transient absorption (fs-TA) spectroscopy to study the dynamics of electronic excitations in self-assembled Ag^+-nucleobase nanostructures for the first time. These systems are attractive for time-resolved study because the excited-state dynamics of nucleobase monomers, oligo- and polynucleotides have been studied extensively since 2000 (see refs. 25-29 for reviews). The accumulated understanding of excited-state deactivation pathways by bare nucleobases in solution and in the gas phase provides a starting point for understanding excited states in metal ion-nucleobase assemblies. These systems may also be suitable models for learning how nucleobase-metal ion interactions affect the photophysics of DNA-bound AgNCs. The AgNCs are partially oxidized, and it has been proposed that nucleobases in the DNA strand

bind to Ag^+ ions located at the periphery of a cluster of Ag(0) atoms.[30] The present study of excited state dynamics of Ag^+-nucleobase assemblies targets understanding of the effects of Ag^+ ion binding on DNA excited states and complements previous transient absorption and fluorescence upconversion studies of DNA-bound AgNCs.[31,32]

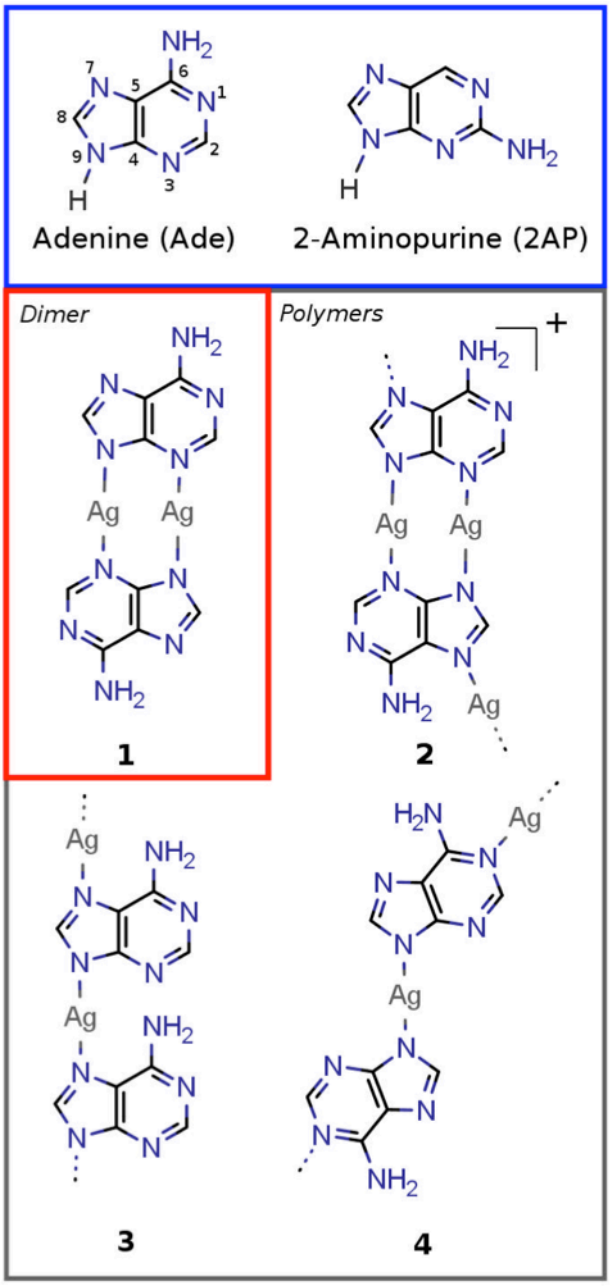

Chart 1. Structures of the nucleobase monomers adenine and 2-aminopurine (top, 9H tautomers are shown) along with representative Ag^+ ion-mediated dimer and polymer structures proposed in the literature: **1** and **2** (ref. 33), 3 (ref. 22), and 4 (ref. 24).

Specifically, we study the electronic absorption spectra and excited-state dynamics in self-assembled nanostructures present in aqueous solutions formed by combining Ag^+ ion with 2-aminopruine (2AP) and adenine (Ade) (see Chart 1) using various optical spectroscopy techniques and AFM imaging. Hereafter, these samples will be referred to as Ag^+/2AP and Ag^+/Ade, respectively. Ade is nearly non-fluorescent in aqueous solution at room temperature (ϕ_f ~3×10^{-4}).[34] In contrast, 2AP is highly fluorescent and has a lifetime of 9.89 ns at 25 °C in room-temperature aqueous solution.[35] The two lowest energy tautomers of Ade in aqueous solution have ultrashort excited state lifetimes of ~0.2 ps and ~8 ps.[36]

The very different photophysical properties of these isomers, Ade and 2AP, and their common ability to serve as building blocks in Ag^+-nucleobase nanoassemblies are the inspiration for our investigation. We are interested chiefly in the intrinsic photophysics of these assemblies, but a further aim is to ascertain what structural information can be won from spectroscopic measurements. Studies of excited-state dynamics in multichromophoric, nanoscale assemblies can potentially reveal information about local structures because excited-state quenching is strongly influenced by species in the immediate environment of a localized excitation.

Experimental

Sample Preparation and Characterization

2-aminopurine (≥ 99%), adenine (≥ 99%), poly(A), D_2O (99.9 % D) and silver nitrate (≥ 99%) were purchased from Sigma-Aldrich, and acetonitrile was obtained from Fischer Scientific. All

chemicals were used as received. Aqueous solutions were prepared using ultrapure, 18.2 MΩ cm water from a water purifier (EMD Millipore). The ratio of the Ag^+ ion concentration to that of nucleobase (β = [Ag^+]/[nucleobase]) was fixed at 2 for all solutions studied except when the Ag^+ ion concentration was varied. Unless otherwise stated, concentrations throughout this paper are formal concentrations equal to the number of moles of a given substance dissolved in water divided by the final solution volume. The value β = 2 was chosen because of previous studies that used the same ratio.[24,33,37,38]

The Ag^+/nucleobase solutions studied were thermally annealed by heating at 90 °C for 5 minutes and cooling to room temperature prior to study. However, the solutions for all measurements made as a function of β were not thermally annealed. The solutions were not pH buffered to avoid precipitating insoluble silver salts. Because protons are released from the nucleobase when Ag^+ ions are added, the actual solution pH for the unbuffered Ag^+/nucleobase solutions was acidic and close to 3.0 for the β = 2 solutions containing 1 mM nucleobase used in the fs-TA experiments.

Steady-state UV-visible (UV-vis) absorption spectra were recorded on solutions held in a 1 mm path length fused silica cuvette. Steady-state emission spectra were recorded in reflection mode with a commercial fluorometer (Horiba/PTI QuantaMaster 8000) using solutions held in a 100 micron path length cell. These solutions had an absorbance of less than 0.05 at the excitation wavelength of 305 nm.

Measurements of the concentration of free Ag^+ ions were performed with a Mettler Toledo perfectION™ comb Ag/S2 Lemo Combination Electrode. The electrode was calibrated before each run using 10^{-5}, 10^{-4}, 10^{-3}, 10^{-2}, and 10^{-1} M $AgNO_3$ solutions. The solutions were constantly stirred and were allowed to equilibrate for two to three minutes after the addition of

each aliquot of 100 mM aq. $AgNO_3$ before making each reading. The minimum sensitivity of the silver electrode was approximately 5×10^{-6} M Ag^+.

AFM images were obtained using a Bruker AXS Dimension Icon microscope equipped with a TESPA-V2 probe. Drop-cast films were prepared from thermally annealed solutions having the same concentrations used in the TA experiments, but the solution was diluted 10× with ultrapure water immediately before drop casting onto a mica substrate (Tedpella) to reduce the concentration of nanostructures per unit area. The sample was held under a stream of room-temperature nitrogen gas until dry. After drying, the samples were washed once with a stream of H_2O and blown dry a second time with nitrogen gas to remove loosely bound material that causes blurring of the AFM images. Measurements were carried out on drop cast films prepared from solutions maintained at room temperature. Images were processed by median filtering and image flattening using Bruker Nanoscope software. Dimensions were measured by randomly sampling 25 locations in multiple images using the Nanoscope software.

Femtosecond Transient Absorption Spectroscopy

A commercial femtosecond laser system (Astrella, Coherent) supplied 1.6 mJ, 90 fs pulses at a 1 kHz pulse repetition rate to an optical parametric amplifier (TOPAS-Prime, Coherent) for generating 265 or 300 nm pump pulses. The pump was chopped at 500 Hz by a mechanical chopper (Newport) synchronized to the laser, such that every other pulse was blocked. The pump pulse energy was attenuated to 1.5 – 2 μJ using a variable neutral density filter, and the spot size of the pump beam was adjusted to 750 – 850 μm (fwhm) at the sample position using a CaF_2 lens.

The broadband continuum probe in the UV-visible region was generated by focusing <1 μJ of the fundamental into a CaF_2 plate (Newlight Photonics, 5 mm, 001 cut). The continuum was collimated by an off-axis parabolic mirror prior to separating the signal and reference using a beamsplitter. The signal portion was focused on the sample using a second off-axis parabolic mirror. The relative polarization of the pump and probe pulses was set to magic angle (54.7°) for all experiments. The crossing angle between the pump and probe beams was approximately 7°. Both the signal and reference beams were dispersed by a fused silica prism spectrograph onto two CCD detectors (Hamamatsu) housed inside one spectrograph. The spectrograph, detectors, and associated electronics were purchased from Stresing Entwicklungsbüro (Berlin, Germany). The spectrograph was calibrated following the procedure of Megerle et al.[39] with an additional parabolic correction for line curvature or "smile"[40] using a BG-36 filter (Thorlabs) and various interference filters (Andover). Instrument control, data acquisition and processing were performed using LabVIEW software (National Instruments).

All fs-TA measurements were performed on solutions containing 1 mM nucleobase and 2 mM $AgNO_3$ ($\beta = 2$) in a 1 mm path length flow cell (Harrick Scientific) with CaF_2 windows. The temporal resolution of our instrument was estimated by measuring the two-photon absorption signal in neat water generated by one pump photon with a wavelength of 265 nm and a second probe photon from the UV portion of the continuum pulse.[41] The signal, which could be detected from the short wavelength edge of the continuum at 310 nm up to approximately 400 nm, had a full width at half maximum of 250 fs and was nearly independent of probe wavelength.

Global fitting of the fs-TA data was performed using the Glotaran software package.[42] TA spectra from 0.5 ps to 3.5 ns were analyzed using multiexponential functions. The time-zero

signal due to simultaneous absorption of the pump and probe photons were excluded. The reported uncertainties of the lifetimes were 2σ.

Results

Steady-State Spectroscopy

The absorption spectrum of Ag^+/Ade (red curve, Figure 1a) is broader and strongly red-shifted compared to Ade (dashed black curve, Figure 1a). The enhanced absorption seen for Ag^+/Ade below 240 nm is due to nitrate ions. The band maximum (λ_{max}) occurs at 260 nm and 264 nm for Ade and Ag^+/Ade, respectively. The Ag^+/Ade sample absorbs at longer wavelengths than neutral Ade, protonated Ade, or deprotonated Ade (Figure S1).

Adding Ag^+ ions to Ade releases protons, and the hydronium ion concentration calculated as 10^{-pH} M from the measured pH vs. β curve (Figure S2) changes nonlinearly as a function of β (Figure 1b). The curve in Figure 1b was recorded by adding concentrated $AgNO_3$ solution such that the concentration of Ade remained approximately constant at 1 mM. When β = 1, approximately one proton has been released to the solvent for every five nucleobases. When β = 2, the 0.8 mM hydronium ion concentration indicates that ~80% of nucleobases have now been deprotonated.

The concentration of bound Ag^+ ($[Ag^+]_{bound}$) was calculated as the total concentration of added silver nitrate minus the concentration of free Ag^+. The latter concentration was measured with a calibrated silver ion electrode. The ratio of bound silver to the concentration of adenine is graphed vs. β in Figure 1b (blue squares). As the data in Table S1 indicate, the concentration of free Ag^+ ion is negligible when $\beta < 1$, indicating that essentially all Ag^+ ions are bound. Initially,

the ratio shown by the blue markers in Figure 1b increases linearly with a slope of 1, but then reaches a plateau near a value of ~1.4 bound Ag^+ ions per nucleobase when $\beta > 1.5$.

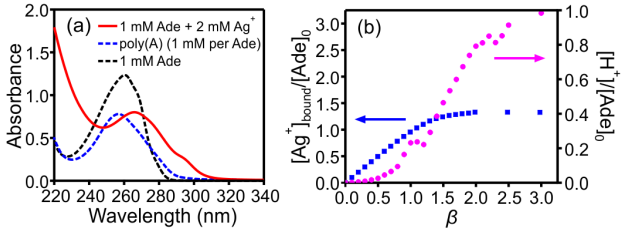

Figure 1. (a) UV-visible spectra of a 2 mM Ag^+/1 mM Ade aqueous solution (red solid line) compared to a 1 mM Ade aqueous solution (black dashed line) and a poly(A) aqueous solution with a per nucleotide concentration of 1 mM (blue dashed line). All spectra were measured in a 1 mm fused silica cell. (b) Bound Ag^+ concentration (blue markers) and released proton concentration (magenta markers) vs. β. The concentration of Ade was held constant at 1 mM.

Adding silver nitrate to 2AP causes its long wavelength absorption band, which is shifted by ~40 nm to longer wavelengths compared to uncomplexed Ade, to shift even further to the red (Figure 2a). λ_{max} is at 305 and 333 nm for 2AP and Ag^+/2AP, respectively (Figure 2a). For reference, the UV-vis spectra of 2AP at three pH values are provided in Figure S3. As observed with Ag^+/Ade, the ratio of $[Ag^+]_{bound}$ to [2AP] plateaus above β = 1.5 (blue markers in Figure 2b), achieving an approximately constant value of 1.5. The concentration of free Ag^+ ion measured with a Ag^+ ion-selective electrode for Ag^+/2AP as a function of β is listed in Table S2. A graph of the concentration of protons released to the solvent for Ag^+/2AP vs. β (magenta markers in Figure 2b) increases sharply between β = 1 and 2 and then changes more slowly, as seen for Ag^+/Ade. The ratio of moles of protons released to moles of 2AP is approximately 0.9 at

$\beta = 2$. Figure S2 shows how pH varies with β. Fluorescence from 2AP is quenched when Ag^+ ion is added to the solution. For the $\beta = 2$ solution, 98% of the emission is quenched (Figure 2c).

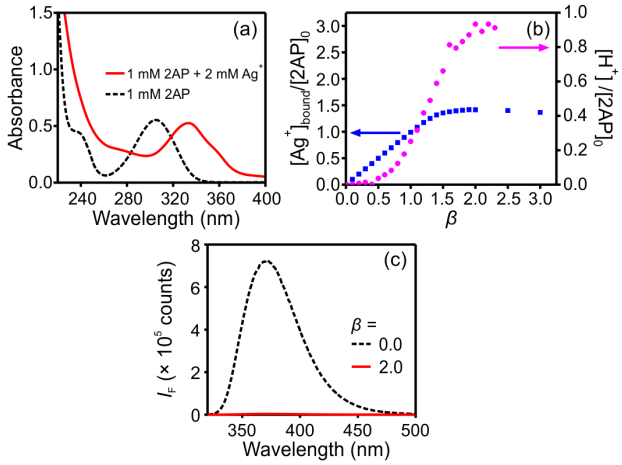

Figure 2. (a) UV-visible spectra of a 2 mM Ag^+/1 mM 2AP aqueous solution (red solid line) and 1 mM 2AP aqueous solution (black dashed line) measured in a 1 mm fused silica cell. (b) Bound Ag^+ concentration (blue markers) and released proton concentration (magenta markers) vs. β measured at a constant nucleobase concentration of 1 mM. (c) Emission spectra of a 2 mM Ag^+/1 mM 2AP aqueous solution (red solid line) and 1 mM 2AP aqueous solution (black dashed line), recorded in a 100 μm fused silica cell in reflection geometry. The concentration of 2AP was held fixed at 1 mM in all experiments.

AFM images of Ag^+/Ade and Ag^+/2AP dried films prepared as described in the experimental section are shown in Figure 3. The Ag^+/Ade sample at room temperature shows a sprawling network of nanofibers that are 30 nm wide on average and > 1 μm long (Figure 3a). Slender nanofibers are also observed in the room temperature Ag^+/2AP sample (Figure 3b).

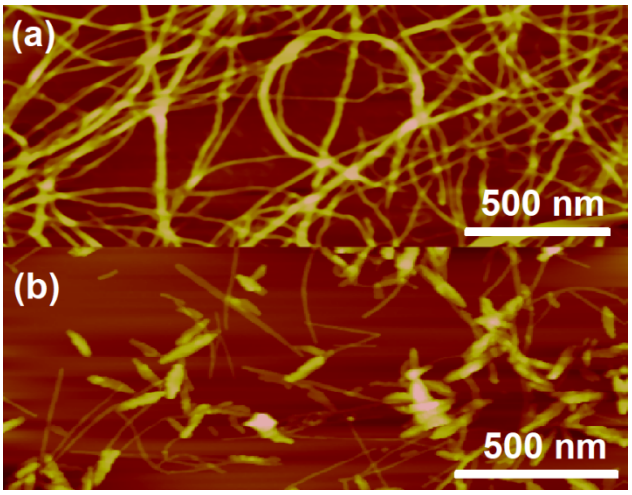

Figure 3. AFM images recorded at room temperature of (a) Ag^+/Ade ($\beta = 2$) and (b) Ag^+/2AP ($\beta = 2$) solutions drop cast on mica after solvent evaporation.

Femtosecond Transient Absorption (fs-TA) Spectroscopy

The fs-TA spectra of Ade, poly(A), and the Ag^+/Ade sample following 265 nm photoexcitation are shown in Figure 4. Global fitting reveals multiexponential decays with time constants of 5.0 ± 0.1 ps, 150 ± 10 ps and > 3 ns (longer than the maximum delay time accessible by our instrument) for the Ag^+/Ade sample (Table 1). The time constants determined for poly(A) from our broadband, UV-vis TA measurements, τ_1=1.3 ± 0.1 ps and τ_2 = 140 ± 10 ps (Table 1), agree well with lifetimes reported by Crespo-Hernández et al.[43] for poly(A) using the single-probe wavelength fs-TA technique (τ_1 = 1.33 ± 0.13 ps and τ_2 = 154 ± 14 ps). The probe wavelength-dependent amplitudes for each exponential decay component define the decay associated difference spectra (DADS), which are shown for each sample on the right side of Figure 4. The transient spectra of Ade and Ag^+/Ade both exhibit a band below 400 nm and a second, broader band between 400 and the limit of our detection window at 660 nm, but differences are evident.

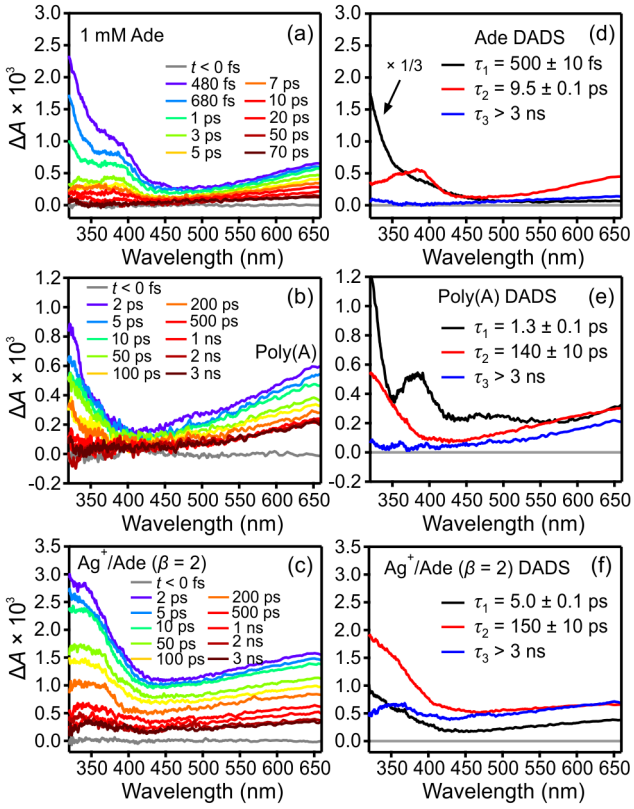

Figure 4. Broadband fs-TA spectra at the indicated delay times for (a) Ade in H_2O at pH 7, (b) poly(A) in H_2O at pH 7, and (c) Ag^+/2AP (β = 2) in H_2O at pH 3 following 265 nm excitation. The Ade concentrations in all solutions were 1 mM. The decay-associated difference spectra (DADS) for Ade, Poly(A) and Ag^+/Ade (β = 2), obtained from global fitting, are shown in panels (d), (e) and (f), respectively. Lifetimes longer than the maximum delay time accessible by our instrument are reported as > 3 ns.

The fs-TA spectra of Ade are similar in appearance to ones published in previous broadband fs-TA studies.[44,45] In addition, the lifetimes obtained from global analysis (Table 1) agree with ones reported previously.[36] Interestingly, the strong positive band seen below 460 nm decays on a subpicosecond time scale, revealing a band centered near 380 nm, which is apparent in the DADS for the 9.5 ± 0.1 ps time constant in Figure 4d. Although 80-100% of the adenine molecules are deprotonated in the Ag^+/Ade assemblies (Figure 1b), TA experiments show that the

excited state population of deprotonated Ade, Ade(–H)$^-$, decays on a subpicosecond timescale and has transient spectral features that differ from those in Ag^+/Ade (Figure S4, Table 1).

Figure 5 compares fs-TA spectra recorded for 2AP at neutral pH and Ag^+/2AP following 300 nm excitation. Table 1 summarizes the best-fit parameters from global fits to a triexponential function. The fs-TA spectrum measured for neutral 2AP with excitation at 300 nm has a broad positive band at approximately 550 nm, accompanied by a weak and narrow band centered at 400 nm (Figure 5a). Similar results were reported in ref. 46 for 2AP excited at 309 nm. In addition, the positive band at 330 nm decays at the same rate as the two bands at longer wavelengths. The overall 2AP signals at neutral pH exhibit a weak picosecond component and a strong nanosecond component (Figure 5a, c) consistent with previous reports.[46-48] The fs-TA spectra of the closed-shell, deprotonated 2AP anion, 2AP(–H)$^-$, collected at pH 12.5 are shown for comparison in Figure S5. The fs-TA spectra of 2AP at pH 2 and corresponding lifetimes from global fitting are shown in Figure S6. The faster decays measured at pH 2 are consistent with the emission quenching of 2AP in acidic conditions reported earlier.[49]

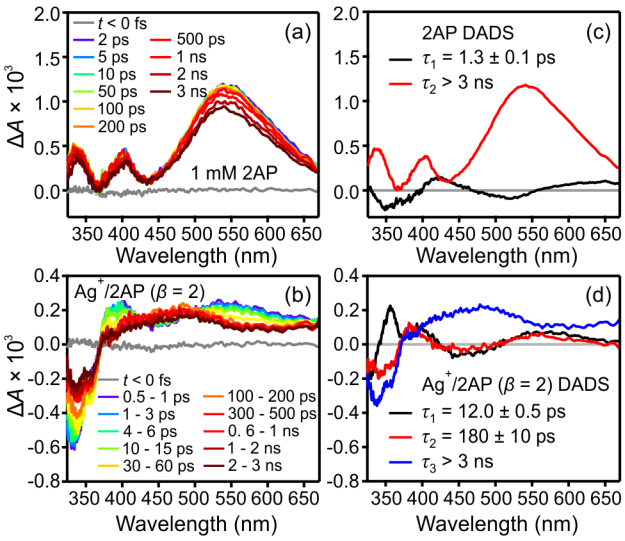

Figure 5. Broadband fs-TA spectra at the indicated delay times for (a) 2AP in H_2O at pH 7, and (b) Ag^+/2AP ($\beta = 2$) in H_2O at pH 3 following 300 nm excitation. The 2AP concentrations in both solutions were 1 mM. Each spectrum in panel (b) was an average of approximately five spectra in the indicated time interval. The decay-associated difference spectra (DADS) for 2AP and Ag^+/2AP (β = 2), obtained from global fitting, are shown in panels (c) and (d), respectively. Lifetimes longer than the maximum delay time accessible by our instrument are reported as > 3 ns.

The fs-TA spectra of the Ag^+/2AP solution (Figure 5b) bear little resemble to those from silver-free 2AP, and the three DADS (Figure 5d) obtained by globally fitting the broadband fs-TA data do not match any of the DADS of free 2AP. Ag^+/2AP absorbs at longer wavelengths than 2AP and negative signals are observed from 320 nm to 360 nm, which are assigned to ground-state bleaching (GSB). According to global analysis, the GSB signals recover with the longest two time constants (i.e., τ_2 and τ_3, see Table 1 and Figure 5d).

In addition to the bleaches below 360 nm, positive bands are seen near 380 nm and 560 nm at short time. These features decay with time constants of 12 ± 0.5 ps and 180 ± 10 ps (Table 1 and Figure 5d), revealing a broad ESA band from 360 nm to 600 nm that persists beyond 3 ns, the longest delay time accessible with our instrument. This broad band is unlike any feature in the fs-TA spectra of uncomplexed 2AP at any pH value.

Table 1. Global Fit Parameters to Broadband Transient Absorption Signals of 2AP and Adenine in the Absence and Presence of Ag^+ Ion.[a]

Sample	pH	τ_1 / ps	τ_2 / ps	τ_3 / ns	λ / nm	$A_1(\lambda)$	$A_2(\lambda)$	$A_3(\lambda)$
2AP	7.0	1.3 ± 0.1	–	> 3 [b]	540	–0.04	–	0.96
$2AP^-$	12	1.5 ± 0.1	–	> 3 [b]	540	0.07	–	0.93
Ag^+/2AP	3.0	12.0 ± 0.5	180 ± 10	> 3 [b]	540	0.24	0.24	0.52
Ag^+/2AP	3.0	12.0 ± 0.5	180 ± 10	> 3 [b]	360	0.37	–0.23	–0.40
Ade	7.0	0.50 ± 0.01	9.5 ± 0.1	> 3 [b]	360	0.77	0.23	<0.01
Ade^-	12	0.60 ± 0.01	–	> 3 [b]	360	0.93	–	0.07
Ag^+/Ade	3.0	5.0 ± 0.1	150 ± 10	> 3 [b]	360	0.22	0.53	0.25
poly(A)	7.0	1.3 ± 0.1	140 ± 10	> 3 [b]	360	0.56	0.36	0.08

[a] Lifetimes (τ_1, τ_2, and τ_3) were determined by globally fitting the broadband fs-TA data at all probe wavelengths to the function, $\sum_{i=1}^{3} a_i(\lambda)\exp(-t/\tau_i)$. The final three table columns show the relative amplitudes defined as $A_i = a_i / \sum_i |a_i|$ at the indicated probe wavelength (λ). Uncertainties are 95% confidence intervals.

[b] Lifetimes greater than the delay time range of the spectrometer are reported as > 3 ns.

Figure S7 compares the kinetic traces at probe wavelengths of 540 nm and 360 nm for 2AP and Ade, respectively, with and without added silver nitrate. The fit parameters are summarized in Table 1. Adding Ag^+ ions dramatically decreases the excited-state lifetime of 2AP, but the opposite trend is observed for Ade. The kinetic trace of poly(A) recorded at 360 nm (green triangles, Figure S7b) appears different at first glance from the decay kinetics of Ag^+/Ade, but global analysis of the broadband data from each sample separately yields similar time constants with different decay amplitudes.

Discussion

Nanoscale Assemblies in Ag^+/Nucleobase Aqueous Solutions

The AFM images in Figure 3 show unequivocally that drop cast films made from the Ag^+/Ade and Ag^+/2AP solutions at room temperature contain nanofibers. Sharma et al.[5] previously described nanofibers in Ag^+-adenine solutions at alkaline pH, but to the best of our knowledge, this is the first report of nanofibers formed by combining 2AP and Ag^+ ions. Sharma et al.[5] observed a hydrogel when 0.8 mL of 100 mM Ade in pH 10.5 aqueous solution was mixed with 1.0 mL of 100 mM aqueous silver nitrate. Electron microscope images of the xerogel produced by freeze drying revealed a tangled network of nanofibers 20 to 35 nm in diameter and several microns long.[5] Our fibers are very similar despite the much lower Ade concentration and higher β value (2.0 vs. 1.25) of our sample. Importantly, our measurements of silver ion binding show that above β = 1.5, there is little additional binding of silver ions at our nucleobase concentration of 1.0 mM. We also note that β = 1 solutions of Ag^+/Ade and 2AP/Ade yield fs-TA signals (Figure S8) and nanofibers (Figure S9) that are very similar to those seen in β = 2 conditions.

An important question is whether the desolvated structures in the AFM images are actually present in solution. Sharma et al.[5] observed nanofibers when the Ade concentration was decreased by an order of magnitude with β = 1.25, conditions that yielded a turbid solution, and not a hydrogel. The concentration of nanofibers in the more dilute solution is likely too low to allow gelation. This evidence that nanofibers form in Ag^+/Ade solutions with millimolar Ade concentrations and β values between 1 and 2 supports our conclusion that the AFM images made using the drop cast films capture the structures present in solution.

Drying can concentrate reagents leading to aggregates or other structures that are not present in dilute solution. However, the results in refs. 23,24 provide strong evidence that polymerization occurs even in highly dilute Ag^+/Ade solutions and is not an artifact of drying. Matsuoka et al.[23,24] detected pronounced linear dichroism from Ag^+/Ade solutions subjected to a flow for an adenine concentration of 79 μM and β values of between 1.4 and 2.2. Extended structures with one dimension greater than approximately 50 nm are required for flow orientation, and Matsuoka et al.[23,24] concluded that long, linear coordination polymers are formed in their dilute solutions.

Excited-state dynamics and evidence of π-stacking in the nanofibers

When Ade is organized into a single strand, characteristic decay times ranging between 100 and 200 ps have been observed in di-,[50,51] oligonucleotides,[50] and homopolymers.[43] Previous studies on single- and double-stranded DNA have shown that the long-lived excited states that last tens to hundreds of picoseconds are excimers or exciplexes with significant charge transfer character that only form when bases are stacked.[52-55] These states are thought to form by photoinduced electron transfer on an ultrafast time scale and decay via charge recombination in the Marcus inverted region.[27]

The fs-TA spectra of Ag^+/Ade resemble those of poly(A) in shape (Figure 4). Specifically, the DADS of the 150 ± 10 ps component of the Ag^+/Ade sample closely resembles that of the 140 ± 10 ps component of poly(A) (compare the red traces in Figure 4e, f). Compared to Ag^+/Ade, the TA signals for poly(A) exhibit a more rapid increase toward the longer wavelength region. This is due to the fact that the poly(A) signal is significantly weaker than that of

Ag^+/Ade, and the solvated electron signal due to 2-photon ionization of the solvent makes a greater contribution to the total TA signal.

We propose that the common excited-state spectrum and decay kinetics observed for Ag^+/Ade and poly(A) are due to excimer formation between π-stacked Ade residues in both systems. Specifically, the absorption band below 450 nm, even though it is partially clipped by the short wavelength detection limit of our ultrafast spectrometer, agrees well with the spectrum of the adenine radical cation ($A^{\bullet+}$),[56] one of the two radical ions present in an excimer state that has strong charge transfer character. Ade stacked with itself is likely responsible for this absorption in both systems, although metal binding may contribute to the somewhat broader band shape in Ag^+/Ade. We have no information about the precise stacking geometry, but fs-TA experiments on several diadenosines in which the two nucleobases are joined by flexible linkers show that the excimer lifetimes are insensitive to the precise base stacking motif and rotational setting of the π-stacked bases.[51]

The Ag^+/2AP results also support the conclusion that π-stacked structures are present. Although 2AP and Ade both act as ligands toward Ag^+ ions and form self-assembled nanostructures, they differ starkly in their photophysics and electronic structure.[57] 2AP emission is strongly quenched in DNA strands by base stacking, making it a useful probe of conformational dynamics in nucleic acids.[58] Figure 2c shows that the fluorescence quantum yield of the $\beta = 2$ Ag^+/2AP solution is much lower than that of uncomplexed 2AP. Furthermore, the excited-state decay of the Ag^+/2AP solution changes from the nearly monoexponential decay with a lifetime of ~10 ns seen for free 2AP[35] to multiexponential decays with a prominent 180 ± 10 ps component not observed in the monomer (Table 1 and Figure 5). Time-correlated single

photon counting (TCSPC) experiments reveal multiexponential fluorescence decay kinetics in UV-excited dinucleotides containing 2AP and Ade.[35]

The Ag^+/Ade and poly(A) signals have similar spectra and τ_2 is approximately 150 ps for both. Despite these similarities, differences are apparent. The long time signal component has greater relative amplitude (A_3 in Table 1) in Ag^+/Ade than in poly(A). In addition, the fastest decay component (τ_1 in Table 1) is almost four times shorter in poly(A) than in Ag^+/Ade and accounts for 56% vs. 22% of the overall signal amplitude (A_1 in Table 1). The equilibrium constant that describes stacking in $(dA)_{18}$ is ~2 at room temperature, implying that stacked domains are only a few bases long at room temperature.[50] Under these conditions, approximately 30% of bases are unstacked, and monomer-like excited states localized on these bases are thought to be responsible for the prominent ~2 ps decay component seen at a probe wavelength of 250 nm for excitation at 266 nm.[50] Similar results are expected for the homopolymer poly(A).

In the Ag^+/Ade sample, Ade bases could be free and uncomplexed, or they could be present in extended assemblies, where they might experience a greater or lesser degree of stacking with other Ade bases. If free, uncomplexed bases were present in the Ag^+/Ade solutions, then a subpicosecond component similar to the τ_1 component of the Ade monomer should be observed. The absence of such a component in Ag^+/Ade together with this sample's stronger excimer component suggest that the amount of free Ade is negligible. Instead, all nucleobases are likely to be integrated into nanofibers containing stacked nucleobase domains that facilitate excimer formation. Similarly, the fluorescence data show very strong fluorescence quenching (> 98%) when 2 mM of Ag^+ ion is added to 1 mM of 2AP, suggesting that the upper limit of unbound 2AP in Ag^+/2AP is 2%. This is consistent with the observation that the fs-TA spectrum of Ag^+/2AP differs from that of free 2AP at all times between 0 and 3 ns (Figure 5), which

indicates that most, if not all, 2AP molecules are organized into Ag^+-containing supramolecular assemblies at room temperature. These observations implicate extensive π-stacking in the Ag^+/2AP and Ag^+/Ade nanostructures.

The origin of the τ_1 component of the Ag^+/Ade solution (5.0 ± 0.1 ps) is uncertain at this time. One possibility is that the initially formed excitonic state decays on a subpicosecond time scale either to an excimer state or to a second excited state, which could be localized on a single base, and which subsequently decays via internal conversion to the ground state, albeit at a rate that is one order of magnitude slower than what is observed for the free base (5 ps vs. 0.5 ps, see Table 1). Computational studies have suggested that steric and other environmental effects present in single- and double-stranded DNA oligonucleotides decrease the rate of internal conversion by an excited state localized on a single base.[59,60] Experimental support for this hypothesis comes from measurements on rigid DNA hairpins showing that there are excited states in well-stacked base sequences that decay faster than excimers.[61]

A further difference in the poly(A) vs. Ag^+/Ade signals concerns the slowest decay component (τ_3). This nanosecond component in the Ag^+/Ade signals accounts for approximately 25% of the observed signal decay at 360 nm, but is three times weaker in poly(A) (Table 1). We considered the possibility that the Ag^+/nucleobase nanostructures yield triplet states due to enhanced intersystem crossing. Rahn and Landry[62] observed fluorescence quenching and a nearly 20-fold enhancement of phosphorescence from poly(rA) with one Ag^+ ion per nucleobase at 77 K in an ethylene glycol-water glass at pH 7, which they attributed to intersystem crossing enhanced by a heavy atom effect. Here, the τ_3 DADS of Ag^+/2AP has little in common with the literature absorption spectrum of the lowest triplet state of 2AP (Figure S10), which has a

pronounced peak at 480 nm.[63] The same conclusion holds for Ag^+/Ade (Figure S11). On this basis, we feel it is unlikely that the longest-lived DADS is due to triplet-triplet absorption.

In addition to the lack of spectral agreement, the τ_3 lifetime is not what is expected for a nucleobase-localized triplet state. In water, the triplet state of 2AP has a ~1 μs lifetime at millimolar concentrations,[63] but the triplet lifetime is concentration dependent due to self-quenching with ground-state 2AP.[64] This suggests that any triplet state would be quenched in much less than 1 ns in Ag^+/2AP nanofibers in light of the extensive π-stacking between 2AP residues. These results suggest that intersystem crossing is either unimportant, or that the lowest triplet state of the assemblies has little in common with the corresponding state of the free nucleobase.

Although the results of this study argue strongly for π-π stacking among the purine bases in the nanofibers present in Ag^+/nucleobase solutions, it is not yet possible to conclude whether stacks occur parallel or perpendicular to the filament direction. To date, the morphologies of self-assembled structures of guanine and guanine derivatives have been studied in greatest detail.[4,65] In fibers made from quartets of guanosine molecules, so-called G wires, individual nanofibers only ~3 nm in diameter are believed to form bundles with stacking parallel to the strand direction.[66] G-ribbons are known in which guanines are extensively hydrogen bonded in two-dimensional sheets.[4] AFM imaging indicates that the resulting structures are ~20 nm wide, but only 1 nm high.[67] However, these structures typically form in non-aqueous solvents, conditions that favor hydrogen bonding over base stacking. For this reason, we speculate that the bases are stacked with their planes normal to the fiber direction as in G wires, but supporting evidence is needed.

Ag^+ binding sites and structural complexity

Determining the microscopic binding motifs that give rise to the self-assembled structures formed between Ag^+ and purine nucleobases is challenging. First, Ade and its constitutional isomer 2AP each have five nitrogen atoms that are potential binding sites. Computational studies confirm that structures with the Ag^+ ion bound to different tautomeric forms of the nucleobase are similar in energy.[68-71] Second, the presence of two or more binding sites per Ade molecule allows coordination oligomers and polymers to form that may be extensively cross-linked. The counterions may also affect the possible structures, but this goes beyond the scope of the present study. We note that crystals formed from adenine and Ag^+ ions at low pH have incorporated perchlorate[72] or nitrate ions.[73] In the mass spectrometry experiments of Vrkic et al.,[33] charged species containing a bound nitrate ion were observed. Third, the AFM images from this study indicate that nanofibers form with Ade or 2AP even though the most favored Ag^+ ion binding sites likely differ for the two isomers. For example, steric crowding by the amino group in the latter has been proposed to inhibit Ag^+ ion coordination to N3.[74]

Although we do not have a detailed structural model, our measurements of quantities such as the number of bound silver ions and the charge per nucleobase can be meaningfully compared to structures proposed in the literature. Vrkic et al.[33,38] studied Ag^+/Ade complexes by mass spectrometry coupled with electrospray ionization, and proposed that linear polymers form, which are built of cross-linked dimers (structures **1** and **2** in Chart 1), a concept inspired by the observation of similar motifs in structures of crystals obtained from acidic aqueous solution.[73,75] Sharma et al.[5] suggested that deprotonated Ade units are joined into linear polymers by N7-Ag^+-N9 linkages (**3** in Chart 1) with individual chains joined by hydrogen bonds with bridging water

molecules. In contrast, Matsuoka et al.[24] favored linear polymers in which deprotonated adenine molecules are connected by repeating N1-Ag^+-N1 and N9-Ag^+-N9 linkages (**4** in Chart 1).

The measured ratio of $[Ag^+]_{bound}$ to nucleobase concentration is 1.3 and 1.4 for our $\beta = 2$ solutions of Ag+/Ade and Ag+/2AP, respectively. These values are close to, but not quite as large as, the value of 1.5 in hypothetical structure **2** in Chart 1. Significantly, the $\beta = 1$ solution also forms nanofibers similar in appearance to those in the $\beta = 2$ solution, and both solutions have similar transient spectra, but the ratio of $[Ag^+]_{bound}$ to the nucleobase concentration when $\beta = 1$ is close to unity, the value characteristic of structures **3** and **4** in Chart 1. These estimates assume that all of the nucleobase in solution is fully bound into nanoassemblies, but we have not seen evidence of a significant concentration of uncomplexed nucleobase for the 1 mM nucleobase solutions with $\beta = 1$ or 2, as discussed above. Based on these findings, it is difficult to choose among the proposed structures in Chart 1.

Structures **2** – **4** in Chart 1 all depict the loss of one proton per nucleobase, but as already noted, only one of every four to five nucleobases has lost a proton in the $\beta = 1$ Ag^+/nucleobase solution. When $\beta = 2$, the ratio of protons released per nucleobase approaches unity, but is still somewhat smaller (0.8 for Ade and 0.9 for 2AP, according to Figures 1b and 2b). Because the stability of nanofibers in aqueous solution is expected to depend sensitively on the presence of charges that prevent aggregation and ensure colloidal stability, we also considered the charge per nucleobase estimated from the number of bound silver ions minus the number of released protons. For the $\beta = 1$, Ag^+/Ade solution, the charge per nucleobase is +0.8, decreasing to +0.5 for the $\beta = 2$ solution. Results for the Ag^+/2AP solutions are similar. We note that the charge per nucleobase is +0.5 for structure **2** in Chart 1, but zero for structures **3** and **4**.

This last point may appear to favor structure **2** over structure **3** or **4**, but it is important to point out that the latter structures could bind additional protons at the pH ~3 conditions of the measurements. A proton displaced when a Ag^+ ion binds to nitrogen does not have to be released to the solvent, but can instead be transferred to a second heteroatom, thereby stabilizing a new tautomeric form of the base. For example, the proton released from N9 binds at N7 or N1 in the acid crystal structures of adenine with Ag^+ ions.[72,73] Adding additional protons to structures **3** or **4** would decrease the protons released to the solvent and increase the charge per nucleobase in better agreement with experiment.

Figures 1b and 2b provide additional insight into the coupling between Ag^+ binding and proton release. In Ag^+/Ade, for example, moving from $\beta = 1$ to 2 increases the concentration of $[Ag^+]_{bound}$ by 0.3 mM, while the concentration of released hydronium ions increases by 0.6 mM. This indicates that Ag^+ ions partially replace protons present in the nanofibers above $\beta = 1$, causing the ratio of $[Ag^+]_{bound}$ to [Ade] to increase, and the pH to drop. As we discuss next, this change might occur without significantly perturbing the overall structure of the nanofibers.

It would be very desirable to study the morphology, excited-state dynamics, and other properties of Ag^+ ion-nucleobase nanostructures as a function of factors such as β, the nucleobase concentration, temperature, and even the annealing history of the sample, but this goes well beyond the aims of the present study. Any future model must account for the similar nanofibers and transient spectra seen in the $\beta = 1$ and $\beta = 2$ solutions (see Figures S8 and S9). These similarities suggest to us that the underlying coordination polymers could be the same in both cases. Our measurements suggest further that this common structure takes up and releases Ag^+ ions and protons without a significant change in morphology or excited-state dynamics. More study is needed to understand if there are significant changes in microscopic structure as β

is varied for these 1 mM nucleobase solutions, but if a single structure is present at both β values, then it cannot be structure **2** in Chart 1, which has a ratio of $[Ag^+]_{bound}$ to [Ade] of 1.5, while this ratio is ~1 in the $\beta = 1$ solution. Finally, although our focus in this subsection has been on the linear coordination polymers drawn in Chart 1, it is possible that the subunits that assemble into nanofibers have an altogether different topology. A further question to be answered is how the subunits, whatever their precise structure, assemble into nanofibers in a way that results in a high degree of π-π stacking among the constituent nucleobases.

Electronic Structure Considerations

The silver ions not only give rise to the three-dimensional structures observed, but they also influence the electronic structure of the nanoassemblies. Ligand-centered transitions are important in many organometallic complexes with silver(I).[76,77] Computational studies published to date have shown that Ag^+ ion binding can induce red shifts in the $\pi \rightarrow \pi^*$ transitions of Ade.[68,69,71] However, these calculated shifts are modest compared to the significant red shifting seen in the UV-vis spectra (Figures 1a and 2a).

It seems likely that excitonic interactions among nucleobases that are brought into close proximity by the Ag^+ ions will also contribute. G quadruplexes absorb at longer wavelengths than the G monomer,[78] and this effect is not due to electronic interaction as the ions involved (e.g., K^+) lack orbitals close enough in energy to the valence orbitals of the nucleobase. The proposal that Ag^+ ions can contribute indirectly to the electronic structure by virtue of how they position the nucleobases in three-dimensional space is consistent with the new excited-state decay pathways revealed in this study.

Conclusions

We have shown by AFM that Ag^+ binding to Ade and its fluorescent analog 2AP yields self-assembled nanofibers. The fs-TA experiments on Ag^+/Ade and Ag^+/2AP show that neither the transient spectra nor the decay dynamics are similar to those observed from the free nucleobases, Ade and 2AP, in their neutral, protonated, or deprotonated forms. Instead, the spectral and temporal fs-TA signals for Ag^+/Ade and poly(A) show many similarities, suggesting that π-stacking between the nucleobases is the common factor controlling excited-state deactivation. This study thus extends the use of fs-TA spectroscopy for detecting stacked nucleobases, which was first described in ref. 51, to metal-nucleobase frameworks. Just as the stabilization of the DNA double helix is the result of both base pairing and π-π stacking, the latter interaction is certain to be a key driving force for the self-assembly of Ag^+-nucleobase structures in aqueous solution.

Although the microscopic binding motifs are still uncertain, the actual microscopic structures may be less complex than at first thought based on the relatively ordered nanostructures observed in the AFM measurements and on the spectroscopy. Supporting this hypothesis, calculated Raman spectra of various mononuclear complexes of adenine with a single silver ion show that ring stretching modes found between 1400 and 1600 cm^{-1} shift by as much as 10 – 20 cm^{-1} upon silver binding.[71] This could indicate that silver ions bind to the same sites on every nucleobase as structures with heterogeneous binding motifs would be expected to yield a distribution of vibrational frequencies. Calculations predicting vibrational spectra and excited states of π-stacked nucleobases in Ag^+/nucleobase frameworks will be an important next step on the path to fully understanding the structure and electronic structure of silver ion-nucleobase nanoassemblies.

Author Information

Corresponding Author
* Bern Kohler. E-mail: kohler.40@osu.edu. Tel: +1 614-688-2635.

ORCID
Bern Kohler: 0000-0001-5353-1655
Joshua Snyder: 0000-0001-7818-1014

Supporting Information Description

Additional steady-state and time-resolved spectra, pH vs. β curves, AFM images, and tables of the free Ag^+ concentration measured for Ag^+/Ade and Ag^+/2AP samples as a function of β.

Acknowledgements

This work was supported by NSF (CHE-1800471) and by startup funding from The Ohio State University. We thank Christopher Grieco for helpful discussions and suggestions. AFM imaging experiments were carried out with financial support from The Ohio State University Institute for Materials Research.

Conflicts of Interest

There are no conflicts of interest to declare.

References

(1) Verma, S.; Mishra, A. K.; Kumar, J. The Many Facets of Adenine: Coordination, Crystal Patterns, and Catalysis. *Acc. Chem. Res.* **2010,** *43*, 79-91.

(2) Loo, K.; Degtyareva, N.; Park, J.; Sengupta, B.; Reddish, M.; Rogers, C. C.; Bryant, A.; Petty, J. T. Ag^{+}-Mediated Assembly of 5 '-Guanosine Monophosphate. *J. Phys. Chem. B* **2010,** *114*, 4320-4326.

(3) Amo-Ochoa, P.; Zamora, F. Coordination Polymers with Nucleobases: From Structural Aspects to Potential Applications. *Coord. Chem. Rev.* **2014,** *276*, 34-58.

(4) Peters, G. M.; Davis, J. T. Supramolecular Gels Made from Nucleobase, Nucleoside and Nucleotide Analogs. *Chem. Soc. Rev.* **2016,** *45*, 3188-3206.

(5) Sharma, B.; Mahata, A.; Mandani, S.; Sarma, T. K.; Pathak, B. Coordination Polymer Hydrogels through Ag(I)-Mediated Spontaneous Self-Assembly of Unsubstituted Nucleobases and Their Antimicrobial Activity. *RSC Adv.* **2016,** *6*, 62968-62973.

(6) Lippert, B.; Miguel, P. J. S. The Renaissance of Metal Pyrimidine Nucleobase Coordination Chemistry. *Acc. Chem. Res.* **2016,** *49*, 1537-1545.

(7) Lopez, A.; Liu, J. W. Self-Assembly of Nucleobase, Nucleoside and Nucleotide Coordination Polymers: From Synthesis to Applications. *ChemNanoMat* **2017,** *3*, 670-684.

(8) Mohapatra, B.; Pratibha; Verma, S. Directed Adenine Functionalization for Creating Complex Architectures for Material and Biological Applications. *Chem. Commun.* **2017,** *53*, 4748-4758.

(9) Pu, F.; Ren, J. S.; Qu, X. G. Nucleobases, Nucleosides, and Nucleotides: Versatile Biomolecules for Generating Functional Nanomaterials. *Chem. Soc. Rev.* **2018,** *47*, 1285-1306.

(10) Petty, J. T.; Zheng, J.; Hud, N. V.; Dickson, R. M. DNA-Templated Ag Nanocluster Formation. *J. Am. Chem. Soc.* **2004,** *126*, 5207-5212.

(11) Soto-Verdugo, V.; Metiu, H.; Gwinn, E. The Properties of Small Ag Clusters Bound to DNA Bases. *J. Chem. Phys.* **2010,** *132*, 10.

(12) Petty, J. T.; Story, S. P.; Hsiang, J.-C.; Dickson, R. M. DNA-Templated Molecular Silver Fluorophores. *J. Phys. Chem. Lett.* **2013,** *4*, 1148-1155.

(13) Swasey, S. M.; Karimova, N.; Aikens, C. M.; Schultz, D. E.; Simon, A. J.; Gwinn, E. G. Chiral Electronic Transitions in Fluorescent Silver Clusters Stabilized by DNA. *ACS Nano* **2014,** *8*, 6883-6892.

(14) Gwinn, E.; Schultz, D.; Copp, S. M.; Swasey, S. DNA-Protected Silver Clusters for Nanophotonics. *Nanomaterials* **2015,** *5*, 180-207.

(15) Ramazanov, R. R.; Sych, T. S.; Reveguk, Z. V.; Maksimov, D. A.; Vdovichev, A. A.; Kononov, A. I. Ag-DNA Emitter: Metal Nanorod or Supramolecular Complex? *J. Phys. Chem. Lett.* **2016,** *7*, 3560-3566.

(16) Petty, J. T.; Ganguly, M.; Yunus, A. I.; He, C.; Goodwin, P. M.; Lu, Y. H.; Dickson, R. M. A DNA-Encapsulated Silver Cluster and the Roles of Its Nucleobase Ligands. *J. Phys. Chem. C* **2018,** *122*, 28382-28392.

(17) Yin, J. J.; He, X. X.; Wang, K. M.; Xu, F. Z.; Shangguan, J. F.; He, D. G.; Shi, H. Label-Free and Turn-on Aptamer Strategy for Cancer Cells Detection Based on a DNA-Silver Nanocluster Fluorescence Upon Recognition-Induced Hybridization. *Anal. Chem.* **2013,** *85*, 12011-12019.

(18) Zhang, L. B.; Wang, E. K. Metal Nanoclusters: New Fluorescent Probes for Sensors and Bioimaging. *Nano Today* **2014,** *9*, 132-157.

(19) Li, J.; Dai, Y.; Wang, S.; Han, C.; Xu, K. Aptamer-Tagged Green- and Yellow-Emitting Fluorescent Silver Nanoclusters for Specific Tumor Cell Imaging. *Sens. Actuators, B* **2016,** *232*, 1-8.

(20) Wu, J.; Li, N.; Yao, Y.; Tang, D.; Yang, D.; Ong'achwa Machuki, J.; Li, J.; Yu, Y.; Gao, F. DNA-Stabilized Silver Nanoclusters for Label-Free Fluorescence Imaging of Cell Surface Glycans and Fluorescence Guided Photothermal Therapy. *Anal. Chem.* **2018,** *90*, 14368-14375.

(21) Li, J.; Yu, J.; Huang, Y.; Zhao, H.; Tian, L. Highly Stable and Multiemissive Silver Nanoclusters Synthesized in Situ in a DNA Hydrogel and Their Application for Hydroxyl Radical Sensing. *ACS Appl. Mater. Interfaces* **2018,** *10*, 26075-26083.

(22) Gillen, K.; Jensen, R.; Davidson, N. Binding of Silver Ion by Adenine and Substituted Adenines. *J. Am. Chem. Soc.* **1964,** *86*, 2792-2796.

(23) Matsuoka, Y.; Norden, B.; Kurucsev, T. Formation of Silver Adenine Long-Chain Aggregates in Neutral Aqueous-Solution: Study of Flow Linear Dichroism. *J. Chem. Soc.-Chem. Commun.* **1984**, 1573-1574.

(24) Matsuoka, Y.; Nordén, B.; Kurucsev, T. Nucleic Acid-Metal Interactions. III. Complexes of Ag(I) with Adenine and 1-Methyladenine from Studies of UV and IR Dichroic Spectra. *J. Crystallogr. Spectrosc. Res.* **1985,** *15*, 545-560.

(25) Crespo-Hernández, C. E.; Cohen, B.; Hare, P. M.; Kohler, B. Ultrafast Excited-State Dynamics in Nucleic Acids. *Chem. Rev.* **2004,** *104*, 1977-2019.

(26) Middleton, C. T.; de La Harpe, K.; Su, C.; Law, Y. K.; Crespo-Hernández, C. E.; Kohler, B. DNA Excited-State Dynamics: From Single Bases to the Double Helix. *Annu. Rev. Phys. Chem.* **2009,** *60*, 217-239.

(27) Chen, J.; Zhang, Y.; Kohler, B. Excited States in DNA Strands Investigated by Ultrafast Laser Spectroscopy. *Top. Curr. Chem.* **2015,** *356*, 39-88.

(28) Improta, R.; Santoro, F.; Blancafort, L. Quantum Mechanical Studies on the Photophysics and the Photochemistry of Nucleic Acids and Nucleobases. *Chem. Rev.* **2016,** *116*, 3540-3593.

(29) Markovitsi, D. UV-Induced DNA Damage: The Role of Electronic Excited States. *Photochem. Photobiol.* **2016,** *92*, 45-51.

(30) Petty, J. T.; Sergev, O. O.; Ganguly, M.; Rankine, I. J.; Chevrier, D. M.; Zhang, P. A Segregated, Partially Oxidized, and Compact Ag_{10} Cluster within an Encapsulating DNA Host. *J. Am. Chem. Soc.* **2016,** *138*, 3469-3477.

(31) Patel, S. A.; Cozzuol, M.; Hales, J. M.; Richards, C. I.; Sartin, M.; Hsiang, J. C.; Vosch, T.; Perry, J. W.; Dickson, R. M. Electron Transfer-Induced Blinking in Ag Nanodot Fluorescence. *J. Phys. Chem. C* **2009,** *113*, 20264-20270.

(32) Volkov, I. L.; Reveguk, Z. V.; Serdobintsev, P. Y.; Ramazanov, R. R.; Kononov, A. I. DNA as UV Light-Harvesting Antenna. *Nucleic Acids Res.* **2018,** *46*, 3543-3551.

(33) Vrkic, A. K.; Taverner, T.; O'Hair, R. A. J. Mapping Charged Silver(I) Adenine Polymers, $[Ad_x + Ag_y - zH]^{(y-z)+}$, Via Electrospray Ionization Tandem Mass Spectrometry Experiments. *J. Chem. Soc., Dalton Trans.* **2002**, 4024-4034.

(34) Callis, P. R. Electronic States and Luminescence of Nucleic Acid Systems. *Ann. Rev. Phys. Chem.* **1983,** *34*, 329-357.

(35) Remington, J. M.; Philip, A. M.; Hariharan, M.; Kohler, B. On the Origin of Multiexponential Fluorescence Decays from 2-Aminopurine-Labeled Dinucleotides. *J. Chem. Phys.* **2016,** *145*, 155101-10.

(36) Cohen, B.; Hare, P. M.; Kohler, B. Ultrafast Excited-State Dynamics of Adenine and Monomethylated Adenines in Solution: Implications for the Nonradiative Decay Mechanism. *J. Am. Chem. Soc.* **2003,** *125*, 13594-13601.

(37) Matsuoka, Y.; Nordén, B.; Kurucsev, T. Nucleic-Acid Metal Interactions .2. Complexes of Silver(I) with Guanosine and 7-Methylguanine from Studies of Isotropic and Dichroic Spectra. *J. Phys. Chem.* **1984,** *88*, 971-976.

(38) Vrkic, A. K.; Taverner, T.; James, P. F.; O'Hair, R. A. J. Gas Phase Ion Chemistry of Charged Silver(I) Adenine Ions Via Multistage Mass Spectrometry Experiments and DFT Calculations. *Dalton Trans.* **2004**, 197-208.

(39) Megerle, U.; Pugliesi, I.; Schriever, C.; Sailer, C. F.; Riedle, E. Sub-50 Fs Broadband Absorption Spectroscopy with Tunable Excitation: Putting the Analysis of Ultrafast Molecular Dynamics on Solid Ground. *Appl. Phys. B: Lasers Opt.* **2009,** *96*, 215-231.

(40) Gates, D. M. The Prismatic Curvature of Spectral Lines. *Am. J. Phys.* **1952,** *20*, 275-280

(41) Reuther, A.; Laubereau, A.; Nikogosyan, D. N. A Simple Method for the in Situ Analysis of Femtosecond UV Pulses in the Pump-Probe Spectroscopy of Solutions. *Opt. Commun.* **1997,** *141*, 180-184.

(42) Snellenburg, J. J.; Laptenok, S. P.; Seger, R.; Mullen, K. M.; van Stokkum, I. H. M. Glotaran: A Java-Based Graphical User Interface for the R Package Timp. *J. Stat. Software* **2012,** *49*, 1-22.

(43) Crespo-Hernández, C. E.; Kohler, B. Influence of Secondary Structure on Electronic Energy Relaxation in Adenine Homopolymers. *J. Phys. Chem. B* **2004,** *108*, 11182-11188.

(44) Kwok, W.-M.; Ma, C.; Phillips, D. L. Femtosecond Time- and Wavelength-Resolved Fluorescence and Absorption Spectroscopic Study of the Excited States of Adenosine and an Adenine Oligomer. *J. Am. Chem. Soc.* **2006,** *128*, 11894-11905.

(45) Stange, U. C.; Temps, F. Ultrafast Electronic Deactivation of UV-Excited Adenine and Its Ribo- and Deoxyribonucleosides and -Nucleotides: A Comparative Study. *Chem. Phys.* **2018,** *515*, 441-451.

(46) Larsen, O. F. A.; van Stokkum, I. H. M.; Groot, M.-L.; Kennis, J. T. M.; van Grondelle, R.; van Amerongen, H. Electronic States in 2-Aminopurine Revealed by Ultrafast Transient Absorption and Target Analysis. *Chem. Phys. Lett.* **2003,** *371*, 157-163.

(47) Pal, S. K.; Peon, J.; Zewail, A. H. Ultrafast Decay and Hydration Dynamics of DNA Bases and Mimics. *Chem. Phys. Lett.* **2002,** *363*, 57-63.

(48) Larsen, O. F. A.; van Stokkum, I. H. M.; de Weerd, F. L.; Vengris, M.; Aravindakumar, C. T.; van Grondelle, R.; Geacintov, N. E.; van Amerongen, H. Ultrafast Transient-Absorption and Steady-State Fluorescence Measurements on 2-Aminopurine Substituted Dinucleotides and 2-Aminopurine Substituted DNA Duplexes. *Phys. Chem. Chem. Phys.* **2004,** *6*, 154-160.

(49) Ward, D. C.; Reich, E.; Stryer, L. Fluorescence Studies of Nucleotides and Polynucleotides. I. Formycin, 2-Aminopurineriboside, 2,6-Diaminopurineriboside, and Their Derivatives. *J. Biol. Chem.* **1969,** *244*, 1228-1237.

(50) Su, C.; Middleton, C. T.; Kohler, B. Base-Stacking Disorder and Excited-State Dynamics in Single-Stranded Adenine Homo-Oligonucleotides. *J. Phys. Chem. B* **2012,** *116*, 10266-10274.

(51) Chen, J.; Kohler, B. Base Stacking in Adenosine Dimers Revealed by Femtosecond Transient Absorption Spectroscopy. *J. Am. Chem. Soc.* **2014,** *136*, 6362-6372.

(52) Doorley, G. W.; Wojdyla, M.; Watson, G. W.; Towrie, M.; Parker, A. W.; Kelly, J. M.; Quinn, S. J. Tracking DNA Excited States by Picosecond-Time-Resolved Infrared Spectroscopy: Signature Band for a Charge-Transfer Excited State in Stacked Adenine–Thymine Systems. *J. Phys. Chem. Lett.* **2013,** *4*, 2739-2744.

(53) Stuhldreier, M. C.; Temps, F. Ultrafast Photo-Initiated Molecular Quantum Dynamics in the DNA Dinucleotide d(ApG) Revealed by Broadband Transient Absorption Spectroscopy. *Faraday Discuss.* **2013,** *163*, 173-188.

(54) Bucher, D. B.; Pilles, B. M.; Carell, T.; Zinth, W. Charge Separation and Charge Delocalization Identified in Long-Living States of Photoexcited DNA. *Proc. Natl. Acad. Sci. U.S.A.* **2014,** *111*, 4369-4374.

(55) Zhang, Y.; de La Harpe, K.; Beckstead, A. A.; Improta, R.; Kohler, B. UV-Induced Proton Transfer between DNA Strands. *J. Am. Chem. Soc.* **2015,** *137*, 7059-7062.

(56) Candeias, L. P.; Steenken, S. Ionization of Purine Nucleosides and Nucleotides and Their Components by 193-nm Laser Photolysis in Aqueous Solution: Model Studies for Oxidative Damage of DNA. *J. Am. Chem. Soc.* **1992,** *114*, 699-704.

(57) Serrano-Andrés, L.; Merchán, M.; Borin, A. C. Adenine and 2-Aminopurine: Paradigms of Modern Theoretical Photochemistry. *Proc. Natl. Acad. Sci. U. S. A.* **2006,** *103*, 8691-8696.

(58) Jones, A. C.; Neely, R. K. 2-Aminopurine as a Fluorescent Probe of DNA Conformation and the DNA-Enzyme Interface. *Q. Rev. Biophys.* **2015,** *48*, 244-279.

(59) Conti, I.; Altoè, P.; Stenta, M.; Garavelli, M.; Orlandi, G. Adenine Deactivation in DNA Resolved at the CASPT2//CASSCF/Amber Level. *Phys. Chem. Chem. Phys.* **2010,** *12*, 5016-5023.

(60) Lu, Y.; Lan, Z. G.; Thiel, W. Hydrogen Bonding Regulates the Monomeric Nonradiative Decay of Adenine in DNA Strands. *Angew. Chem.-Int. Edit.* **2011,** *50*, 6864-6867.

(61) Chen, J.; Thazhathveetil, A. K.; Lewis, F. D.; Kohler, B. Ultrafast Excited-State Dynamics in Hexaethyleneglycol-Linked DNA Homoduplexes Made of at Base Pairs. *J. Am. Chem. Soc.* **2013,** *135*, 10290-10293.

(62) Rahn, R. O.; Landry, L. C. Ultraviolet Irradiation of Nucleic Acids Complexed with Heavy Atoms. II. Phosphorescence and Photodimerization of DNA Complexed with Silver. *Photochem. Photobiol.* **1973,** *18*, 29-38.

(63) Reichardt, C.; Wen, C. W.; Vogt, R. A.; Crespo-Hernández, C. E. Role of Intersystem Crossing in the Fluorescence Quenching of 2-Aminopurine 2 '-Deoxyriboside in Solution. *Photochem. Photobio. Sci.* **2013,** *12*, 1341-1350.

(64) Wierzchowski, K. L.; Berens, K.; Szabo, A. G. Triplet-Triplet Absorption Studies of Intersystem Crossing Mechanism of 2-Aminopurines. *J. Lumin.* **1975,** *10*, 331-343.

(65) Davis, J. T. G-Quartets 40 Years Later: From 5 '-GMP to Molecular Biology and Supramolecular Chemistry. *Angew. Chem. Int. Ed.* **2004,** *43*, 668-698.

(66) Buerkle, L. E.; Li, Z.; Jamieson, A. M.; Rowan, S. J. Tailoring the Properties of Guanosine-Based Supramolecular Hydrogels. *Langmuir* **2009,** *25*, 8833-8840.

(67) Wang, X.; Zhou, L.; Wang, H.; Luo, Q.; Xu, J.; Liu, J. Reversible Organogels Triggered by Dynamic K+ Binding and Release. *J. Colloid Interface Sci.* **2011,** *353*, 412-419.

(68) Rubina, A. Y.; Rubin, Y. V.; Sorokin, V. A.; Shukla, M. K.; Leszczynski, J. Complexes of Adenine with Metal Ions: Stability and Excited States. *Pol. J. Chem.* **2005,** *79*, 1873-1882.

(69) Schreiber, M.; González, L. A CASPT2 Study of the Excited States of Adenine Tautomers with Silver Ions. *Chem. Phys. Lett.* **2007,** *435*, 136-141.

(70) Schreiber, M.; González, L. Structure and Bonding of Ag(I)-DNA Base Complexes and Ag(I)-Adenine-Cytosine Mispairs: An Ab Initio Study. *J. Comput. Chem.* **2007,** *28*, 2299-2308.

(71) Huang, R.; Zhao, L. B.; Wu, D. Y.; Tian, Z. Q. Tautomerization, Solvent Effect and Binding Interaction on Vibrational Spectra of Adenine-Ag+ Complexes on Silver Surfaces: A DFT Study. *J. Phys. Chem. C* **2011,** *115*, 13739-13750.

(72) Gagnon, C.; Hubert, J.; Rivest, R.; Beauchamp, A. L. Crystal-Structure of Di-Mu-Adeninium-Disilver(I) Perchlorate Monohydrate. *Inorg. Chem.* **1977,** *16*, 2469-2473.

(73) Mishra, A. K.; Prajapati, R. K.; Verma, S. Probing Structural Consequences of N9-Alkylation in Silver-Adenine Frameworks. *Dalton Trans.* **2010,** *39*, 10034-10037.

(74) Mohapatra, B.; Venkatesh, V.; Verma, S. Crystal Engineering with 2-Aminopurine Containing a Carboxylic Acid Pendant. *Cryst. Growth Des.* **2014,** *14*, 5042-5052.

(75) Gagnon, C.; Beauchamp, A. L. Structure Cristalline du Nitrate de *catena*-(μ-Méthyl-9 Adénine) Argent(I) Hydraté. *Acta Crystallogr. Sect. B-Struct. Commun.* **1977,** *33*, 1448-1454.

(76) Kunkely, H.; Vogler, A. Optical Properties of Ag(Tripod)X with Tripod=1,1,1-Tris(Diphenylphosphinomethyl)Ethane and X^- = Cl^- and I^-: Intraligand and Ligand-to-Ligand Charge Transfer. *Inorg. Chim. Acta* **2006,** *359*, 388-390.

(77) Barbieri, A.; Accorsi, G.; Armaroli, N. Luminescent Complexes Beyond the Platinum Group: The d^{10} Avenue. *Chem. Commun.* **2008**, 2185-2193.

(78) Mergny, J. L.; Phan, A. T.; Lacroix, L. Following G-Quartet Formation by UV-Spectroscopy. *FEBS Lett.* **1998,** *435*, 74-78.

TOC Image